ACS OMEGA

Open Access



http://pubs.acs.org/journal/acsodf

Article

# Benzidine Derivatives as Electroactive Materials for Aqueous Organic Redox Flow Batteries

Martha M. Flores-Leonar, Gloria Acosta-Tejada, Humberto G. Laguna, Carlos Amador-Bedolla, Mariano Sánchez-Castellanos,* and Víctor M. Ugalde-Saldívar*

Cite This: *ACS Omega* 2023, 8, 32432−32443

Read Online

ACCESS | Metrics & More | Article Recommendations | Supporting Information

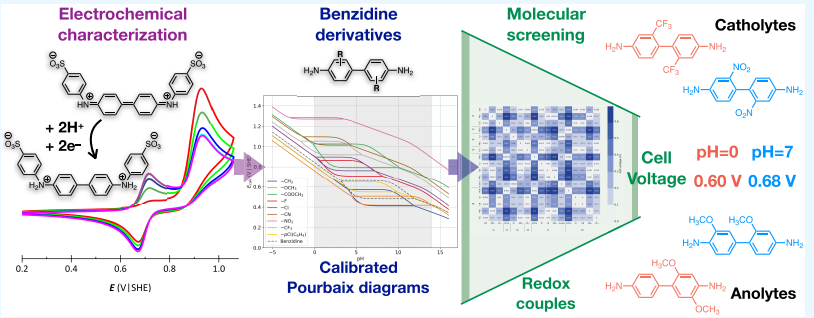


**ABSTRACT:** This paper presents a theoretical and experimental evaluation of benzidine derivatives as electroactive molecules for organic redox flow batteries. These redox indicators are novel electroactive materials that can perform multielectron transfers in aqueous media. We performed the synthesis, electrochemical characterization, and theoretical study of the dimer of sodium 4-diphenylamine sulfonate, a benzidine derivative with high water solubility properties. The Pourbaix diagram of the dimer shows a bielectronic process at highly acidic pH values ($\leq 0.9$) and two single-electron transfers in a pH range from 0 to 9. The dimer was prepared *in situ* and tested on a neutral electrochemical flow cell as a stability diagnostic. To improve cell performance, we calculate and calibrate, with experimental data, the Pourbaix diagrams of benzidine derivatives using different substitution patterns and functional groups. A screening process allowed the selection of those derivatives with a bielectronic process in the entire pH window or at acidic/neutral pH values. Given the redox potential difference, they can be potential catholytes or anolytes in a flow cell. The couples formed with the final candidates can generate a theoretical cell voltage of 0.60 V at pH 0 and up to 0.68 V at pH 7. These candidate molecules could be viable as electroactive materials for a full-organic redox flow battery.

## INTRODUCTION

Redox flow batteries (RFBs) are a viable option to solve solar and wind energy intermittency. In RFBs, the electroactive material is dissolved and pumped through an electrochemical cell, where the charging and discharging processes occur. Traditional flow batteries use transition metals as the active electrolyte, but these metals are expensive, toxic, environmentally unfriendly, and scarce.[1,2] One way to solve these limitations is by using organic compounds as redox-active materials, which are composed of earth-abundant elements, improving safety and cost. Besides, the functionalization of organic cores allows property tuning through different theoretical screening models.

Redox-active electrolytes based on quinones, viologen, TEMPO, phenazine, and alloxazine derivatives are among the most evaluated organic molecules for aqueous redox flow batteries.[3−5] However, only a few anthraquinone, phenazine, and viologen derivatives demonstrated long-term stability.[6,7]

Redox indicators are widely known for their practical use as visual indicators in oxidation−reduction titrations. These materials represent a novel option as they mainly involve multielectron-transfer reactions. Some publications report redox indicators and dyes involving bielectron-transfer processes in RFBs with acceptable efficiencies, such as methylene blue,[8,9] basic red 5,[10] indigo carmine,[11] gallocyanine,[12] and neutral red.[13]

Although benzidine is not itself a redox indicator, certain *N*-substituted and 3,3′-substituted benzidines, naphthidine, 3,3′-substituted naphthidines, and diverse derivatives of these compounds exhibit color changes in a potential range of 0.7−1.1 VlSHE.[14] Benzidine and *N*,*N*′-diphenylbenzidine derivatives can present a redox equilibrium involving the transfer of up to two electrons in aqueous media. Under certain conditions, the

Received: April 5, 2023
Accepted: August 3, 2023
Published: August 31, 2023

**Scheme 1. Synthesis Scheme of the Oxidized Dimer (Dimer-Ox) from SDPAS**

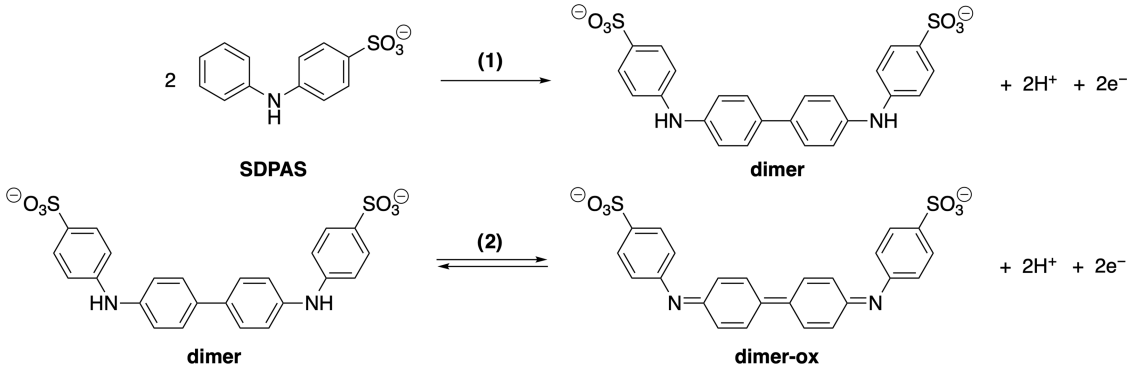


oxidation of benzidine and its derivatives is a reversible process involving the transfer of two electrons and two protons to form the oxidized quinoid structure corresponding to benzidine-4,4′-diimine. However, as already reported by numerous authors, this oxidation−reduction reaction is a complex process and depends significantly on the pH of the medium.[15−17]

Won *et al.* reported a low water solubility for benzidine; thus, water−acetonitrile solutions have been used for their electrochemical characterization instead.[16] In the same study, the authors showed that at pH values lower than 3.5, a concerted bielectronic process is observed, while in a pH range from 3.5 to 10, a two-electron transfer is carried out in monoelectronic steps. On the contrary, basic pH values resulted in undesired phenomena, producing uncharacterized electroactive species.

The compound diphenylamine-4-sulfonic acid has been reported as a redox indicator,[18] involving a two-electron and two-proton reaction that produces the dimeric form (Scheme 1). A further oxidation reaction can occur to the dimer to give the quinoid form (dimer-ox). Due to the sulfonate groups, this derivative is expected to have better water solubility than benzidine.

This work presents the experimental and theoretical study of the dimer prepared *in situ* by electrosynthesis at different pH values, electrochemical characterization, Pourbaix diagram (PD) analysis, and stability test performed in a redox flow cell. The starting material was the commercial reagent sodium 4-diphenylamine sulfonate (SDPAS). To get the oxidized dimer (dimer-ox) derived from SDPAS, we investigated the synthetic route in two steps: (1) a homocoupling in para-position to the aniline group to form a dimer and (2) an electro-oxidation to form dimer-ox.

Given the electrochemical properties reported for benzidine, we consider monoelectronic-transfer processes in the theoretical study of the dimer. Finally, a theoretical screening of benzidine derivatives is discussed based on their PD, calibrated with the experimental results. Some molecules exhibited dismutation processes, which allowed the selection of possible catholytes or anolytes to propose new candidates for an organic redox flow battery.

## METHODOLOGY

**Experimental Methods.** *Cyclic Voltamperometry.* Electrochemical characterization was carried out with a potentiostat−galvanostat model PGSTAT 100 N. Each measurement used a glassy carbon microelectrode as a working electrode after it was polished with a diamond suspension (1 $\mu$m) and cleared with deionized water. A platinum (Pt) wire was used as a counter electrode and an AgCl−Ag electrode was used as a reference (0.26 V|SHE). A scan rate of 0.1 V $s^{-1}$ was used to obtain cyclic voltamerograms (CVs), referenced with respect to the standard hydrogen electrode (SHE).

For the experimental PD, different pH solutions were used: $HClO_4$ 1 mol $L^{-1}$ pH = 0.35 and 0.00, $HClO_4$ 2 mol $L^{-1}$ pH = −0.30, 1.00, 2.00, 3.00, 4.00, and 5.00, $HClO_4$ 8 mol $L^{-1}$ pH = −0.90, $HClO_4$ 10 mol $L^{-1}$ pH = −1.00, $HClO_4$ 12 mol $L^{-1}$ pH = −1.10, $H_2SO_4$ 1 mol $L^{-1}$ pH = 0.35, acetate buffer 1 mol $L^{-1}$ pH = 5.00, phosphate buffer solution 1 mol $L^{-1}$ pH = 7.00, $NH_4OH$ 1 mol $L^{-1}$ pH = 9.00, NaOH 0.001 mol $L^{-1}$ pH = 11.00 and NaOH 0.01 mol $L^{-1}$ pH = 12.00. When required, the pH values were adjusted with NaOH.

*Electrosynthesis and Stability Flow Cell Proof.* Oxidized dimer was obtained by electrosynthesis using an Arbin Instrument Testing System, model MSTAT240441, and a redox flow cell. Posolyte and negolyte solution reservoirs were bubbled throughout the system with $N_2$ and were pumped with a flow rate of 50 mL $min^{-1}$, employing a peristaltic pump. Electrosynthesis was performed using a posolyte tank containing 0.05 mol $L^{-1}$ of SDPAS and a negolyte tank containing 0.25 mol $L^{-1}$ of $[Fe(CN)_6]^{3-}$ both in a phosphate buffer solution 1 mol $L^{-1}$, pH = 7. Dimer stability in a flow cell assay was performed with a 10 $cm^2$ area cell equipped with graphite plates and carbon sheets assembled with Nafion 212 50-$\mu$m thickness membrane soaked in a blank electrolyte. The galvanostatic mode was used, and the imposed current value was 0.05 A.

According to the redox potential values, the concentration of the oxidized dimer was 0.025 mol $L^{-1}$ and 0.125 mol $L^{-1}$ for $[Fe(CN)_6]^{3-}$ and $[Fe(CN)_6]^{4-}$ in the posolyte reservoir, respectively. Charge and discharge cycles were performed by applying a current of ±10 mA in periods of time close to 3000 s. During electrosynthesis, both sides of the cell were characterized by cyclic voltamperometry, using a potentiostat−galvanostat model PGSTAT 100 N, in a conventional three-electrode cell, a glassy carbon as a working microelectrode, Pt wire as a counter electrode, and AgCl−Ag as a reference electrode (0.26 V|SHE); a scan rate of 0.1 V $s^{-1}$ was used to obtain all CVs, referenced with respect to SHE.

**Theoretical Calculations.** *Computational Details.* Geometry optimization started by performing a minimum energy conformer search, and a subsequent geometry optimization with the MMFF94 force field, using the Open Babel 2.4.0 software.[19] The next step was performed with the Gaussian 16 Suite,[20] using the previous coordinates as input for a two-step optimization, first with the PM7 pseudopotential followed by a density functional theory (DFT) with the B3LYP[21] hybrid functional, a 6-311+G(d,p) basis set, and the solvation model based on the density (SMD)[22] in water. A vibrational frequency analysis


https://doi.org/10.1021/acsomega.3c02297
ACS Omega 2023, 8, 32432−32443

**Scheme 2. Proton-Coupled Electron-Transfer (PCET) Diagram for Benzidine Derivatives Containing the Main Species Involved in the First and Second Reduction Processes**[a]

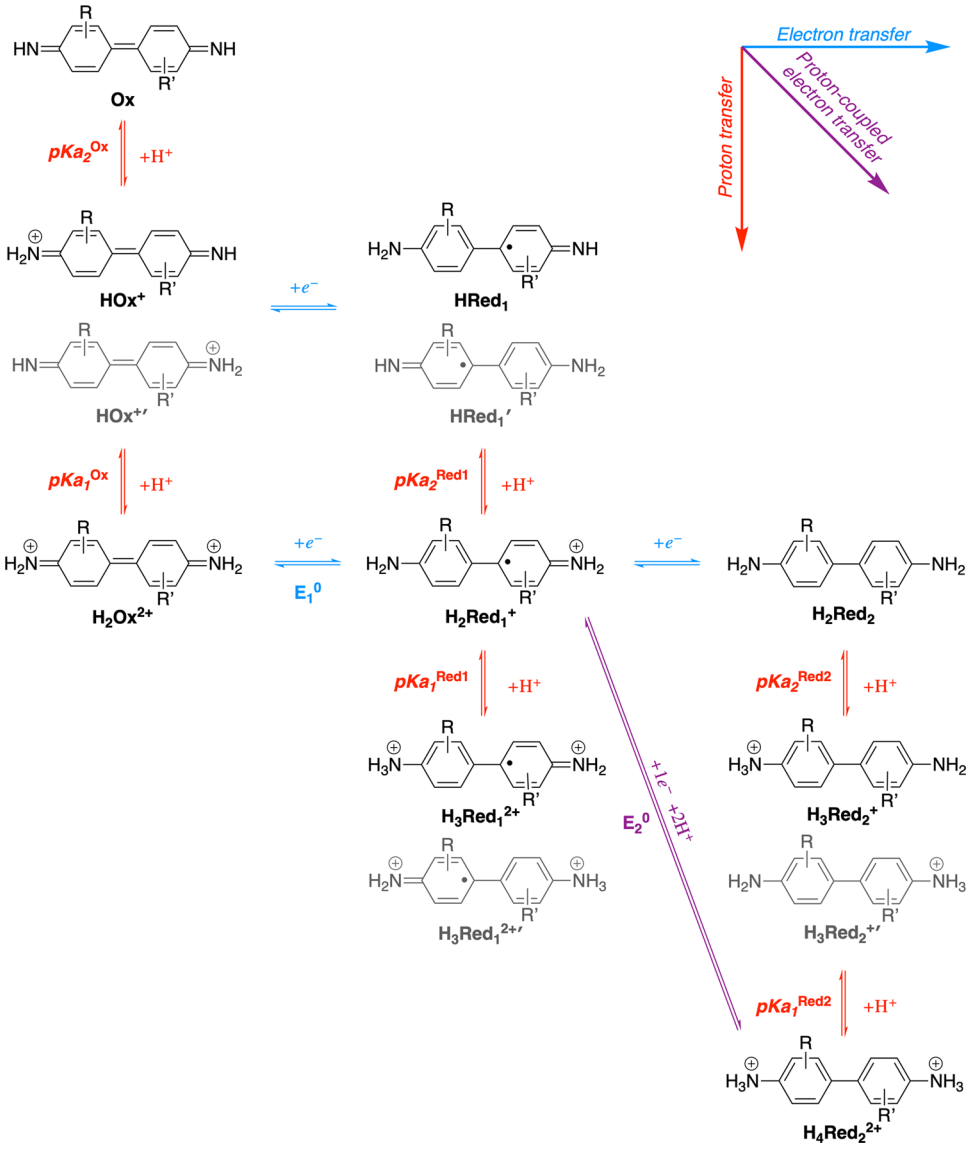


[a]The species in black correspond to symmetric derivatives, while the species in gray show up for nonsymmetric substitutions.

confirmed the existence of an energy minimum. Finally, we obtained the Gibbs free energy for further property calculations.

Calculation of the reduction potentials and acid dissociation constants is very sensitive to small variations of the computed free energies; for that reason, the minimum energy conformers should be accurate. In our experience, the procedure described guarantees the accuracy of these computations.

*Redox Potential and p$K_a$ Calculations.* The p$K_a$ computation for the oxidized and reduced species is necessary to build the pH predominance zone diagram (PZD)[23] and specify the principal redox equilibria. For a dissociation reaction of the HA species in solution (eq 1), the Gibbs free-energy difference ($\Delta G^0_{HA}$) is related to the acid dissociation constant ($K_a$) and its respective p$K_a$ through eq 2. The $\Delta G^0_{HA}$ value is calculated, in turn, through eq 3, where the $G(H^+)$ value was set to −269 kcal mol$^{-1}$[24,25]

$$HA_{(s)} \rightleftarrows A^-_{(s)} + H^+_{(s)};\ \Delta G^0_{HA} \quad (1)$$

$$pK_a = \frac{\Delta G^0_{HA}}{2.303RT} \quad (2)$$

$$\Delta G^0_{HA} = G(A^-) + G(H^+) - G(HA) \quad (3)$$

With the principal redox equilibria, we computed their standard reduction potential ($\Delta E^0_{Ox/Red}$). In general, for a reaction involving the transfer of $n$ electrons and $m$ protons (eq 4), the $\Delta E^0_{Ox/Red}$ is calculated using eq 5, where $F$ is Faraday's constant and SHE is the absolute potential for the standard hydrogen electrode in water (4.44 V) used as reference.[26] The change in Gibbs free energy ($\Delta G^0_{Ox/Red}$) shown in eq 6 considers the free energy of the $m$ protons, where we can note that in the particular case of $m = 0$, the equation reduces to a pure electron transfer

$$Ox_{(s)} + ne^- + mH^+_{(s)} \rightleftarrows H_mRed^{(m-n)}_{(s)};\ \Delta G^0_{Ox/Red} \quad (4)$$



https://doi.org/10.1021/acsomega.3c02297
ACS Omega 2023, 8, 32432−32443

$$E^0_{Ox/Red} = \frac{\Delta G^0_{Ox/Red}}{-nF} - SHE \quad (5)$$

$$\Delta G^0_{Ox/Red} = G(H_mA^{(m-n)}) - G(A) - mG(H^+) \quad (6)$$

For the benzidine derivatives studied (Scheme 4 in the Results and Discussion section), we considered the proton-coupled electron-transfer diagram shown in Scheme 2. The horizontal and vertical reactions correspond to pure electron and proton transfers, respectively, whereas a proton-coupled electron-transfer reaction (PCET) is depicted in the diagonal. The structures shown in gray are additional protonated species generated due to the molecule symmetry (depending on the substitution pattern). For the p$K_a$ calculation, we considered these additional species and selected the proton transfer reaction with the highest p$K_a$ value.

From the p$K_a$ values, we built the PZDs to obtain the predominant equilibria for all derivatives calculated. At pH = 0, these equilibria correspond to eqs 7 and 8, which are in agreement with the PZD for the SDPAS dimer

$$H_2Ox^{2+} + e^- \rightleftarrows H_2Red_1^{\bullet+};\ E_1^0 \quad (7)$$

$$H_2Red_1^{\bullet+} + 2H^+ + e^- \rightleftarrows H_4Red_2^{2+};\ E_2^0 \quad (8)$$

Finally, the standard redox potentials ($E_1^0$ and $E_2^0$) were calculated according to the described methodology.

*Pourbaix Diagrams.* A plot of the redox potential as a function of pH is called the Pourbaix diagram. To compute PD, we used the Nernst eq 9 to calculate the conditional reduction potential ($E'_{Ox/Red}$) for a specific reduction equilibrium. In this equation, $E^0_{Ox/Red}$ is the standard reduction potential, $R$ is the gas constant, $T$ is the temperature, and $Q$ is the reaction quotient. Writing $Q$ in terms of the acidity constants, we obtain eqs 10 and 11 (shown in the Electrochemical Characterization section), and these equations are pH-dependent functions used to plot the PDs of benzidine and its derivatives

$$E'_{Ox/Red} = E^0_{Ox/Red} + \frac{RT}{nF}\ln Q \quad (9)$$

## RESULTS AND DISCUSSION

**Electrochemical Characterization.** *Electrosynthesis.* According to the synthetic route in Scheme 1, the global reaction involves four protons and four electrons. In this work, the oxidized dimer was synthesized at a final concentration of 0.025 mol $L^{-1}$. The posolyte tank corresponds to 0.05 mol $L^{-1}$ of SDPAS and the negolyte tank to 0.25 mol $L^{-1}$ of $[Fe(CN)_6]^{3-}$, both in phosphate buffer solution and 1 mol $L^{-1}$ pH = 7 (or in some cases, other buffer solutions were employed). First, CVs of each reservoir were obtained, and then a positive oxidation current was applied in the SDPAS posolyte side. The CVs obtained for each electrolyte solution are listed in Figure 1. An irreversible oxidation peak of SDPAS at $E_{ap}$ = 0.89 V|SHE was observed in the CV started in the positive direction (Figure 1a); for the negolyte tank solution, a reversible reduction peak at $E_{cp}$ = 0.17 V|SHE was observed in the CV started in the negative direction (Figure 1b), and the corresponding oxidation signal appears at $E_{ap}$ = 0.64 V|SHE.

Figure 2 shows two oxidation processes of SDPAS in the CV started in the positive direction (brown line); first, an oxidation peak at $E_{ap}$ = 0.89 V|SHE was observed, which indicates that the monomer is being transformed into the dimer, and a second oxidation peak appears at $E_{ap}$ = 0.48 V|SHE, just at the end of

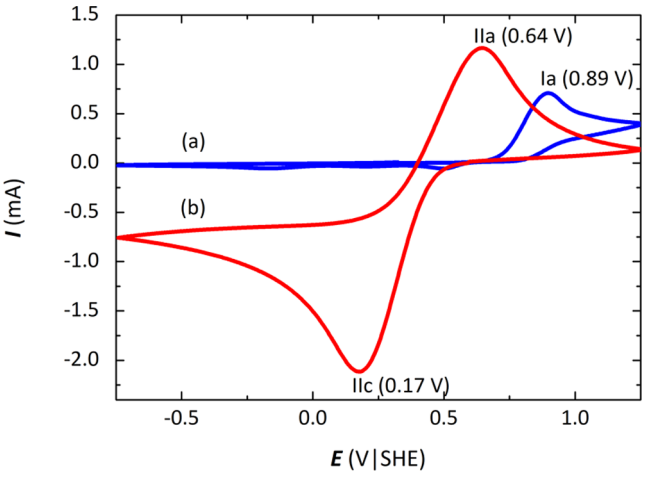


**Figure 1.** Initial CVs of each reservoir in positive scan and negative scan: (a) 0.05 mol $L^{-1}$ of SDPAS (blue line) and (b) 0.25 mol $L^{-1}$ of $[Fe(CN)_6]^{-3}$ (red line), respectively.

CV. On the other hand, a new reduction peak, $E_{cp}$ = 0.01 V|SHE, appears in an inverse scan (Figure 2a) since the dimer has a lower reduction potential; the imposition of potential to which the system is subjected also favors the dimer oxidation. The conversion of the monomer to the oxidized dimer is reached when the oxidation signal ($E_{ap}$ = 0.89 V|SHE) disappears almost completely; at the same time, the reduction signal at 0.01 V|SHE increases as well as the corresponding oxidation signal at 0.48 V|SHE; these signals represent the redox process of the dimer. The final CV (Figure 2b, purple line) shows only the reduction and oxidation signals of the dimer. Simultaneously, in the other half of the cell, $[Fe(CN)_6]^{3-}$ was reduced to $[Fe(CN)_6]^{4-}$.

To observe the changes after electrosynthesis in the posolyte tank, the CVs presented in Figure 3 show the isolated reduction ($E_{cp}$ = 0.01 V|SHE) and oxidation signals ($E_{ap}$ = 0.48 V|SHE) of the dimer after electrosynthesis.

The peak potential difference value of the dimer is $\Delta E_p$ = 470 mV, which is a *quasi*-reversible system. This electrosynthesis process was performed at different pH values to obtain the PD and characterize the redox processes.

The electrochemical characterization of the dimer through cyclic voltamperometry (CV) was incorporated in the Supporting Information (Figure S1). The CV was extended up to 50 cycles for a 0.02 mol $L^{-1}$ monomer solution with 1.0 mol $L^{-1}$ of sulfuric acid. In the Supporting Information, Figure S2 shows the voltamperogram of the solution after some time of CV experimentation, showing that the signals are different from those of the SDPAS dimer produced chemically ($HClO_4$ with hydrogen peroxide 70%) or electrochemically, which gives evidence of the formation of a different compound.

In Figure S3, the $^1$H NMR of the SDPAS dimer obtained by $H_2O_2$ chemical oxidation shows that it is not possible to identify the characteristic signals of the compound chemically synthesized because of the amount of water present and the strongly acid pH of the reaction medium. The voltamperogram incorporated in the Supporting Information (Figure S4) of the chemically synthesized compound depicts only the characteristic oxidation and reduction peaks of the dimer, demonstrating that only this product is formed and is the same as that obtained after 15 CV cycles in the electrode interface. We also observe an intense color that demonstrates the high degree of conjugation of the oxidized dimer species as proposed in Scheme 1.


https://doi.org/10.1021/acsomega.3c02297
ACS Omega 2023, 8, 32432−32443

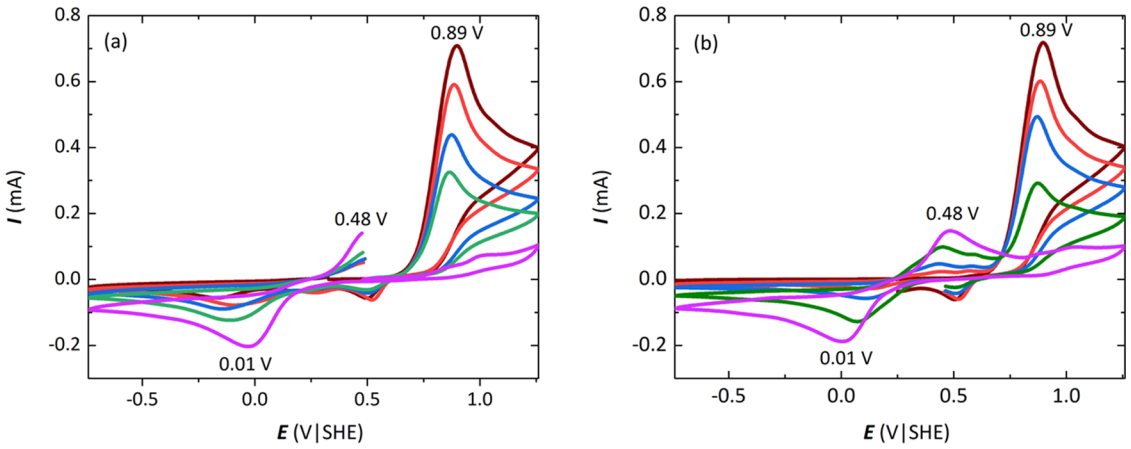


**Figure 2.** CVs of the electrosynthesis process to convert SDPAS to dimer: (a) positive and (b) negative directions at 0.1 V $s^{-1}$.

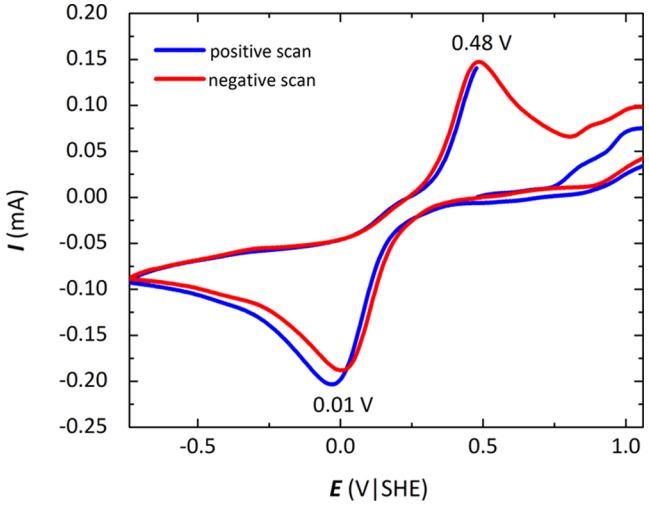


**Figure 3.** CVs to positive (blue line) and negative (red line) scans of the reduction of the oxidized dimer and its corresponding oxidation after the electrosynthesis process.

Additionally, the monomer-to-dimer conversion is not completed through the CV technique because this experiment involves electrode−solution interface phenomena and not bulk solution phenomena. In order to show this, we perform a CV experiment after 10 cycles; then, the solution was stirred in order to spread the product formed in the interface and then the CV was obtained; this is shown in Figure S5 of the Supporting Information.

Finally, Figure S6 shows the CVs for the addition of $H_2O_2$ to a 0.05 mol/L solution of SDPAS in $HClO_4$ 70% m/m; this demonstrates that only a compound is obtained with this chemical reaction and corresponds to the dimer-ox. This process validates the electrochemical technique to characterize the dimer species at different pH values.

*Pourbaix Diagram for the Oxidized Dimer.* To construct the experimental PD, studies were carried out in diverse solutions at different pH values. The dimer was obtained in two different ways; the first one was by electrosynthesis, using a redox flow cell (taking about 220 min), where SDPAS is completely converted into oxidized dimer and its characterization was done using voltamperograms. The second method was *in situ*, on a glassy carbon microelectrode, performing cyclic voltammetry with at least 25 cycles and using a scan speed of 0.1 V $s^{-1}$. Both techniques showed similar results, corroborated by the dimer signals (Supporting Information, Figure S7). Therefore, cyclic voltammetry resulted in a cleaner method and was used to minimize the conversion time to oxidize the monomer into an oxidized dimer. Some solutions such as $H_2SO_4$ presented ionic-pair interactions with the oxidized dimer (which was confirmed by the less positive redox potential), so their results were discarded in the construction of the PD. The most consistent results were obtained with perchloric acid solutions. Figure 4a exemplifies this process in $HClO_4$ at different pH values when pH ≤ −0.9 (Figure 4b); there is a reversible wave at $E_{cp-I}$ = 0.67 V|SHE and its corresponding oxidation signal at $E_{ap-I}$ = 0.71 V|SHE. The potential difference between the anodic and cathodic peaks ($\Delta E_p$) is 40 mV, which means that the redox process involves an exchange of two electrons per dimer molecule; consequently at these conditions, the dismutation of the radical species for the dimer occurs. However, at −0.9 < pH ≤ 2 (Figure 4c), two reduction processes coexist, one at a half-wave potential of $E_{1/2}$ = 0.56 V|SHE and another at $E_{1/2}$ = 0.72 V|SHE. This indicates that the radical species of the oxidized dimer is stable, and the reduction electron transfer occurs in two monoelectronic steps, each process with $\Delta E_p$ = 60 mV. When the values are 3 ≤ pH ≤ 5 (Figure 4d), the first reduction signal, $E_{cp-I}$, overlaps to the second reduction peak, $E_{cp-II}$, and the peak potential difference becomes smaller (approx. 100 mV), which could indicate that the dimer dismutes again at higher pH values.

On the other hand, in solutions at pH ≥ 5, the system is unstable; the value of $\Delta E_p$ increases considerably, greater than 300 mV (see the Supporting Information, Figure S8a,b); this represents a loss of reversibility. When the pH of the solution is more alkaline (pH ≥ 9), the cyclic voltamperograms (see the Supporting Information, Figure S8c,d) show the appearance of new peaks, which suggests the formation of new electroactive species, making difficult the characterization at these pH values, as previously reported by Won et al.[16] for benzidine. Therefore, the stabilization zone of the radical species and the dismutation is at −1.1 ≤ pH ≤ 2.[27]

$E_{1/2}$ and $\Delta E_p$ for the first redox process (Ia−Ic) are presented in Table 1. It can be seen that when $\Delta E_p$ is near 0.03 V, a concerted bielectronic process occurs, while an increment of $\Delta E_p$ to 0.06 V evidences a reversible monoelectronic process. The $E_{1/2}$ values do not show a dependence on pH from 0 to 2; however, at higher pH (≥5), this one decreases in the same way as the benzidine behavior reported by Won et al.[16] (see Figure S8 in the Supporting Information).


https://doi.org/10.1021/acsomega.3c02297
ACS Omega 2023, 8, 32432−32443

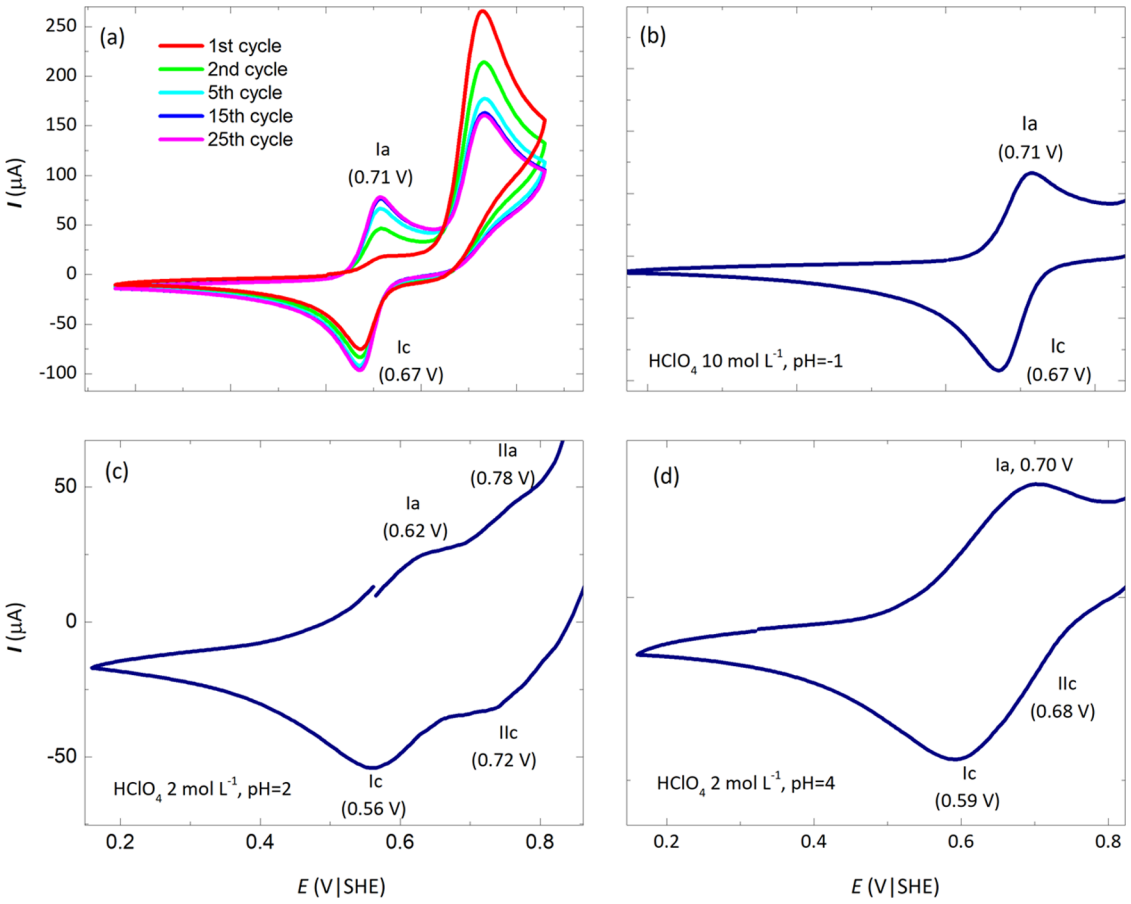


**Figure 4.** CVs of the electrosynthesis process to convert SDPAS to dimer in perchloric acid at different pH values: (a, b) pH = −1, (c) pH = 22, and (d) pH = 4; at 0.1 V $s^{-1}$.

**Table 1. $E_{1/2}$ and $\Delta E_p$ Values of Benzidine Derivatives in Different Solutions and under Different pH Conditions for the First Redox Process (Ia−Ic)**

| pH | solution | conc. (mol $L^{-1}$) | $\Delta E_p$ (V\|SHE) | $E_{1/2}$ (V\|SHE) |
|---|---|---|---|---|
| −1.10 | $HClO_4$ | 12 | 0.11 | 0.75 |
| −1.00 | $HClO_4$ | 10 | 0.04 | 0.69 |
| −0.90 | $HClO_4$ | 8 | 0.05 | 0.69 |
| −0.30 | $HClO_4$ | 2 | 0.09 | 0.48 |
| 0.00 | $HClO_4$ | 1 | 0.09 | 0.48 |
| 0.35 | $H_2SO_4$ | 1 | 0.09 | 0.52 |
| 1.00 | $HClO_4$ | 2 | 0.09 | 0.48 |
| 2.00 | $HClO_4$ | 2 | 0.06 | 0.75 |
| 3.00 | $HClO_4$ | 2 | 0.13 | 0.65 |
| 4.00 | $HClO_4$ | 2 | 0.11 | 0.65 |
| 5.00 | $HClO_4$ | 2 | 0.11 | 0.65 |
| 5.00 | acetate buffer | 1 | 0.38 | 0.37 |
| 7.00 | phosphate buffer solution | 1 | 0.47 | 0.25 |
| 9.00 | $NH_4OH$ | 1 | | |
| 11.00 | NaOH | 0.001 | | |
| 12.00 | NaOH | 0.01 | | |

To complete the electrochemical characterization, the theoretical PD of SDPAS was obtained at the B3LYP/6-311+G(d,p) level of theory. Scheme 3 shows the one-dimensional (1D) predominance zone diagram with the relevant species for each reduction.

**Scheme 3. One-Dimensional Predominance Zone Diagram for the SDPAS Dimer Species**

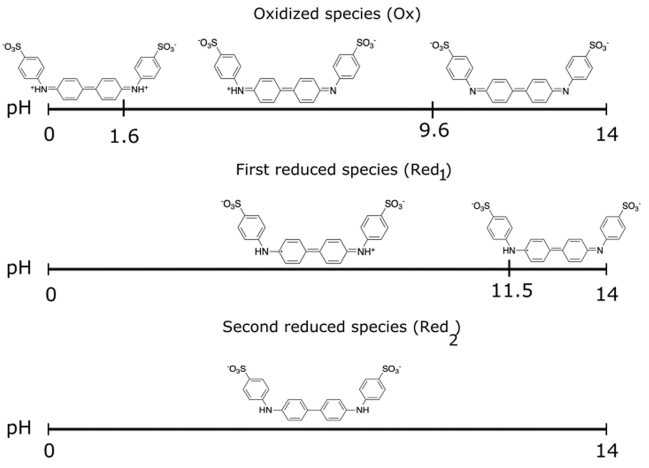


The generalized functions[28] for each reduction in terms of the acid dissociation constants and the standard reduction potential at pH = 0 are:

$$E'_{Ox/Red_1} = E^0_{Ox/Red_1} + 0.06 \log\left(\frac{1 + 10^{(pH - pK_{a1}^{Ox})} + 10^{(2pH - pK_{a1}^{Ox} - pK_{a2}^{Ox})}}{1 + 10^{(pH - pK_{a1}^{Red_1})}}\right) \quad (10)$$



https://doi.org/10.1021/acsomega.3c02297
ACS Omega 2023, 8, 32432−32443

$$E'_{\mathrm{Red}_1/\mathrm{Red}_2} = E^0_{\mathrm{Red}_1/\mathrm{Red}_2} + 0.06\log(1 + 10^{(\mathrm{pH}-\mathrm{p}K_{a1}^{\mathrm{Red}_1})}) \quad (11)$$

The PD obtained with these functions (Figure S9 in the Supporting Information) shows two monoelectronic reduction processes from pH = 0 to 9.2; outside this interval, a bielectronic process is observed. From the experimental results for this compound, it can be noted that at pH below zero, a concerted two-electron reduction process also occurs. To match the theoretical and experimental results, a calibration was performed. This process implied a correction of −0.177 and +0.652 V for the first and second calculated reduction potentials, respectively. Theoretical p$K_a$ values for all of the species involved in the PD were adjusted by 2.85 units. Figure 5 shows a comparison after the fitting. It is observed that, as well as benzidine, the dimer presents undesired phenomena at high pH values, limiting the use of the compound in this range.

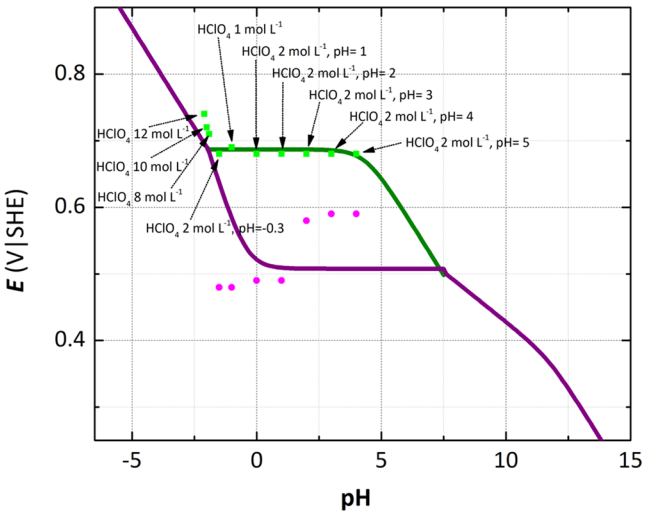


**Figure 5.** Comparison of the theoretical Pourbaix diagram with the experimental potential values in aqueous media of the SDPAS dimer. The green and purple lines correspond to the first and second reduction processes, respectively.

*Stability Flow Cell Proof.* As discussed previously, the stability of this compound was tested in a redox flow cell. The equipment and cell configuration previously mentioned were used. The initial CV values for negolyte and posolyte solutions are shown in Figure 6. The expected voltage for this assembly is $\Delta E$ = 0.18 V as indicated in the corresponding voltampero-grams.

The charge process started by applying +10 mA into the redox flow cell to oxidize the compound on the positive side and −10 mA to reduce the $[Fe(CN)_6]^{3-}$; then, in the discharge step, the inverse process is applied during 21 cycles. Figure 7 shows current and potential values obtained for the first six charge−discharge cycles. The next 15 cycles can be seen in Figure S10 (Supporting Information).

For the stability diagnostic for the dimer, a simple way to evaluate the Coulombic efficiency of the cell is by comparing the amount of electricity that passes during the charge/discharge processes for each of the cycles carried out in the redox flow cell.

The redox flow cell assay showed a charge capacity fade near 5% during the first cycles (Table 2), but the capacity level had significant losses at higher current values and cycles (evidenced in the charge and discharge times decrease). When the cell reaches 21 cycles of operation (Supporting Information, Figure S10), the efficiency drops to 65%.

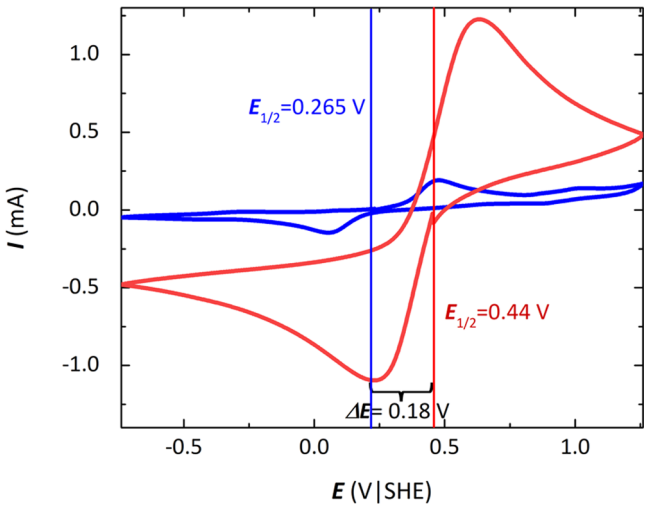


**Figure 6.** Cyclic voltammograms for the oxidation of the oxidized dimer at 0.025 mol $L^{-1}$ (blue line) and $[Fe(CN)_6]^{3-}$ and $[Fe(CN)_6]^{4-}$ at 0.125 mol $L^{-1}$ (red line) at 0.1 V $s^{-1}$.

The evaluated dimer, whose central structure is benzidine, is a new type of compound tested in a flow cell. The obtained results suggest that possible structure modifications could improve the efficiency of these compounds. Therefore, a theoretical screening of different benzidine derivatives is performed in the following section.

**Theoretical Study.** *Pourbaix Diagrams for Benzidine and Benzidine Derivatives.* In this section, we analyze the theoretical PDs of different benzidine derivatives. The goal is to tune their properties, making them more suitable for application as catholytes or anolytes in redox flow batteries.

To perform this study, we consider eight different substitutions on the benzidine backbone (Scheme 4a, S1−S8) and 24 electron-withdrawing or electron-donating functional groups (Scheme 4b,c, R2−R25) in order to obtain different effects on their physicochemical properties. Only single and double substitutions (with the same functional group) were considered to make the derivatives more synthetically accessible. It is worth mentioning that some of the functional groups have acid−base activity, which gives rise to additional species (not considered in Scheme 2). Hence, a richer PZD diagram could be obtained, modifying the resulting PD.

Benzidine molecule (R1 in Scheme 4b) is used as a reference to evaluate the electronic effect of substitutions and functional groups on the redox potential and pH values. The PD for benzidine is shown as a dashed line in each plot (Figures 8 and 9), where we observe three zones. The first one, at pH < 3.1, corresponds to a proton-coupled two-electron reduction, where a dismutation of the free radical occurs. The second zone, at 3.1 < pH < 11.9, is characterized by two successive one-electron reduction reactions; therefore, a predominance zone of the free radical is present. The equilibria involved are electron transfer and proton-coupled electron transfer. Finally, at pH > 11.9, a proton-coupled two-electron reduction occurs once again. However, the latter interval has a disadvantage, that is, the presence of different and noncharacterized species, as reported in previous experiments.[16]

Exploration of different benzidine derivatives aims to increase the two-electron reduction zone beyond pH ≈ 3. This target can


https://doi.org/10.1021/acsomega.3c02297
ACS Omega 2023, 8, 32432−32443

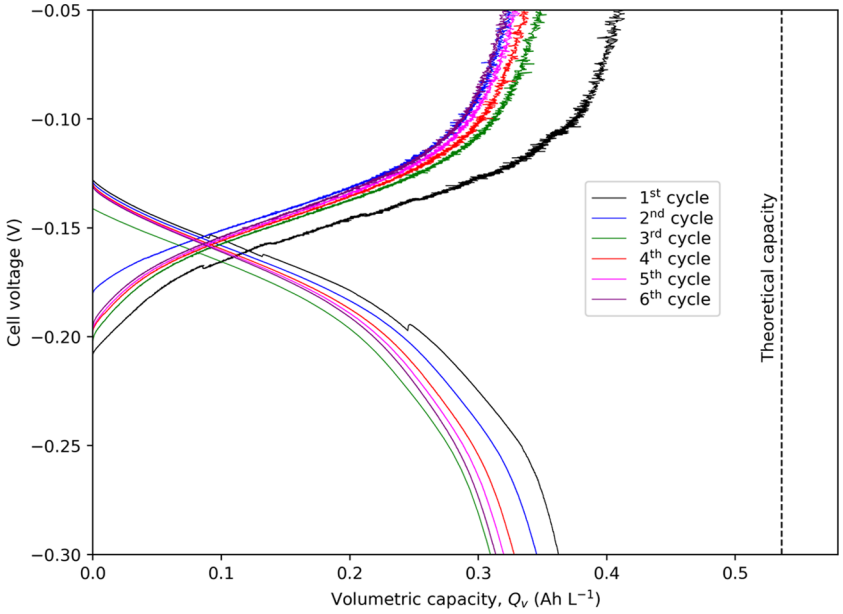


**Figure 7.** Volumetric capacity of cycling of the oxidized dimer in a redox flow cell proved at 10 mA.

**Table 2. Coulombic Efficiency (CE) and Charge−Discharge Times Evaluated for the Dimer in the Flow Cell**

| cycle | 1 | 2 | 3 | 4 | 5 | 6 |
|---|---|---|---|---|---|---|
| charge time (s) | 3477 | 2909 | 3111 | 3039 | 2965 | 2886 |
| discharge time (s) | 3277 | 3040 | 2966 | 2949 | 2885 | 2829 |
| CE (%) | 94.24 | 104.5 | 95.3 | 97.0 | 97.3 | 98.00 |

be reached by following different strategies. On the one hand, increasing the p$K_a$ of the two-electron-reduced species would result in a displacement of the free-radical dismutation zone toward higher pH values, hence increasing the proton-coupled-two-electron-transfer zone in the PD. On the other hand, tuning the first and second reduction potentials (for instance, decreasing the first and increasing the second) would leave a small or negligible stability window and thus a larger dismutation zone of the free radical. Additionally, an overall increase or decrease in the reduction potentials could lead to more suitable applications of these derivatives as posolytes or negolytes.

PDs for all substitutions where the functional group is nonacid−base-active are in the Supporting Information, Figure S11a−h. Most cases, depending on the functional group, preserve the free-radical predominance zone. However, there are a few combinations of substitution and functional groups where the dismutation at all pH intervals (the shading zone in each plot) prevails over the radical stability zone.

**Scheme 4. (a) Substitution Patterns (S1−S8) Considered for Benzidine Derivatives. (b) Functional Groups without Acid−Base Activity (R1−R10). (c) Functional Groups with Acid−Base Equilibria (R11−R25)**

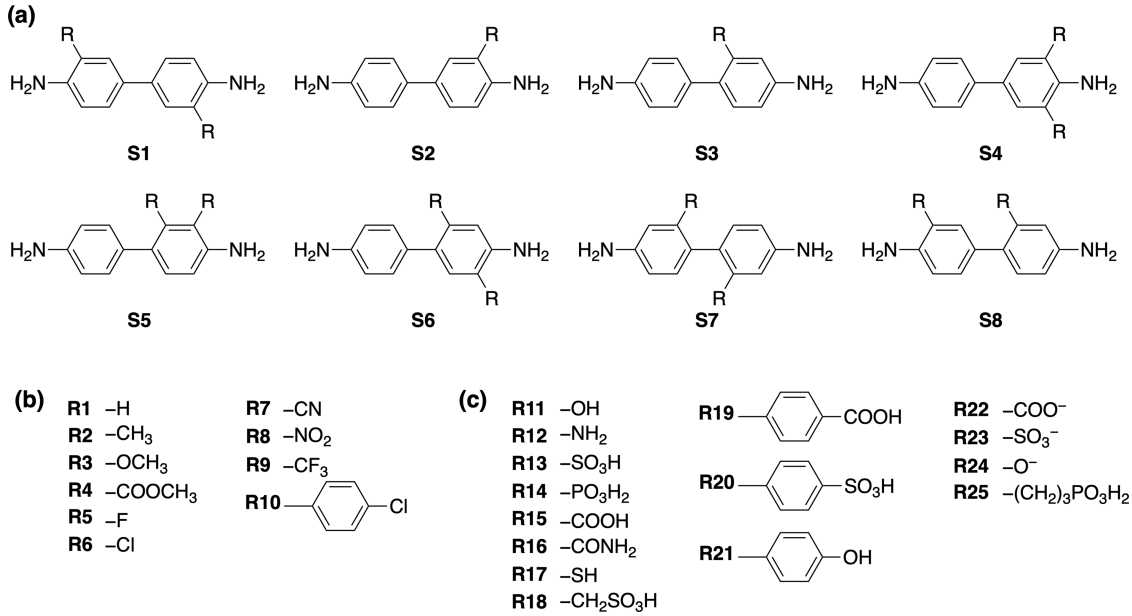




https://doi.org/10.1021/acsomega.3c02297
ACS Omega 2023, 8, 32432−32443

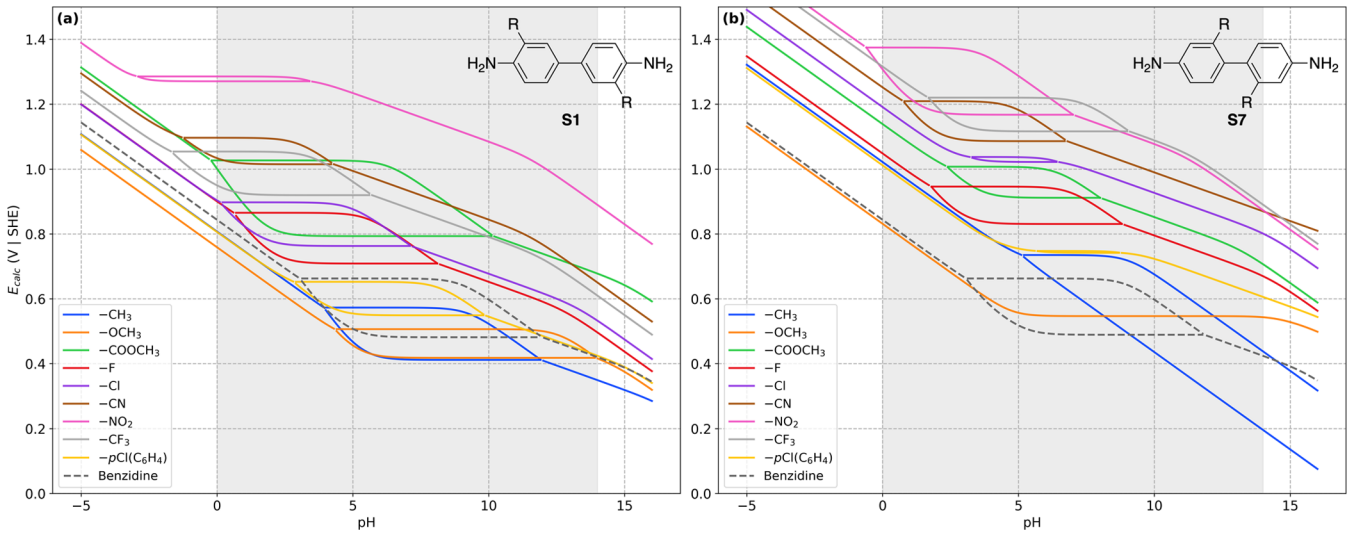


**Figure 8.** Pourbaix diagrams for nonacid−base functional groups with a specific substitution pattern. (a) Substitution pattern S1. (b) Substitution pattern S7. Benzidine is shown as a reference in dashed lines. The shading zone corresponds to the conventional water pH window.

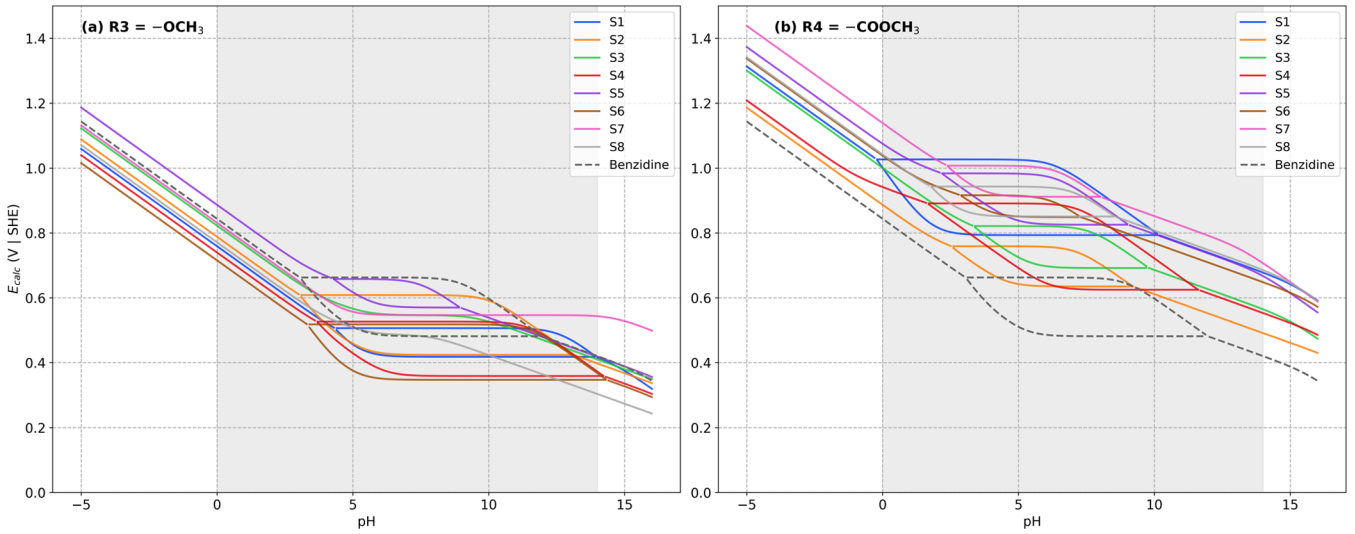


**Figure 9.** Pourbaix diagrams for a specific functional group R with all substitution patterns (S1−S8). (a) R3 = $-OCH_3$ functional group. (b) R4 = $-COOCH_3$ functional group. Benzidine is shown as a reference in dashed lines. The shading zone corresponds to the conventional water pH window.

Substitutions S1 and S7 (Figure 8a,b) with the $-NO_2$ and $-OCH_3$ groups, respectively, are examples of these effects; note that S1 has functional groups (R) in 3,3′-benzidine positions, while S7 are 2,2′-benzidine substitutions. These diagrams were calibrated according to the methodology described for the dimer (see the discussion around Figure 5). In both substitutions, when the redox potential difference between the first and second reductions is small, the dismutation of the radical species is favored. However, when the difference becomes significant, the stability zone of the radical species emerges. In most cases, this stability zone appears at low pH values. Substitution S7 increases the redox potential since there is shifting in the PDs toward more positive values. For a specific substitution, the redox potential also depends on the electron-withdrawing or electron-donating functional group. The former displaces the redox potential toward higher values, while the latter displaces the redox potential toward lower values. To highlight this electronic effect for all substitutions studied (S1−S8), Figure 9 is presented for derivatives R3 = $-OCH_3$ (electron-donating) and R4 = $-COOCH_3$ (electron-withdrawing). We can notice that redox potentials are higher for R4 derivatives than the R3. Finally, the derivatives (combination of substitution pattern and functional group) presenting a full dismutation or slight stability window in the whole water pH window are S3−R3, S7−R3, S8−R3, S7−R10, S7−R6, and S1−R8.

From the above discussion, derivatives showing a dismutation in the whole pH range are desirable for their application as electrolytes in RFBs. In the cases where the radical stability window is present, derivatives can be selected if the window has a small redox potential difference or preferably begins beyond neutral pH, leaving the dismutation zone at acidic pH. This would lead to the operation of a flow cell with still soft conditions (pH from 0 to 7).

A set of functional groups not yet discussed corresponds to Scheme 4c (R11−R25), which could have additional acidity constants not considered in the PD. Hence, its interpretation must be careful. An example of the resulting PDs for this set of functional groups is shown in Figure S12 in the Supporting Information for substitution S1. As an approximation to describe the influence of the acid−base properties on the PD and figure


https://doi.org/10.1021/acsomega.3c02297
ACS Omega 2023, 8, 32432−32443

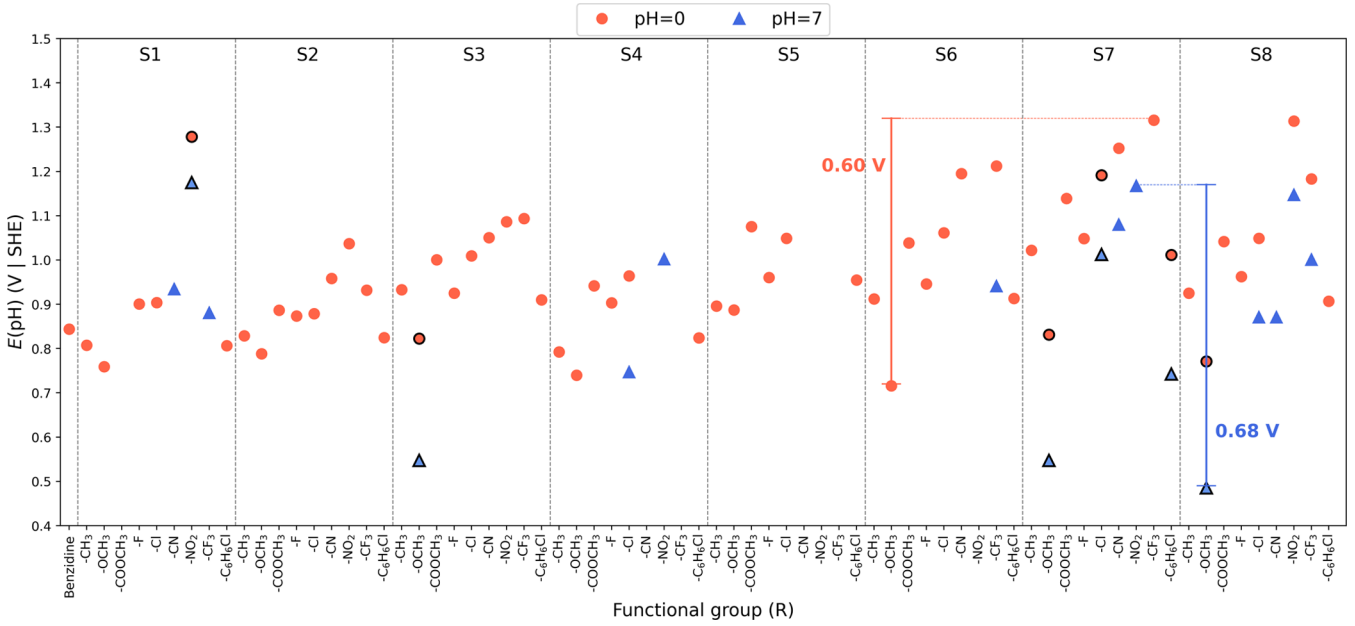


**Figure 10.** Conditional reduction potential at pH = 0 and pH = 7 for the derivatives screened exhibiting a bielectronic reduction process. Derivatives exhibiting dismutation in the entire water pH window are enclosed in black.

out an improved diagram, we can look at the derivatives R22 = $-COO^-$, R23 = $-SO_3^-$, and R24 = $-O^-$ and their respective protonated species R11 = −OH, R13 = $-SO_3H$, and R15 = −COOH. The PDs for these acid−base pairs are in Figure S13a−f, where we can see significant changes in both the redox potential and the radical stability window. We can intuitively consider that a better PD would have an intermediate aspect between these two extremes. However, to rigorously include the effects of the acid−base equilibria, the equations to build the PD must depend on the associated acidity constant. We will evaluate these effects in future studies.

Based on the previous analysis, we establish two selection criteria to perform a screening of benzidine derivatives as potential electrolytes for RFBs: (1) derivatives with a bielectronic process or small stability window of the radical species in the entire water pH window (0−14); (2) derivatives with a dismutation process below neutral pH (0−7) and a stability window of the radical species beyond neutral pH. We did not consider the derivatives at basic pH nor with acid−base activity in the screening for the reasons explained above.

The reduction potential of the screened molecules exhibiting the bielectronic process at pH = 0 and 7 is depicted in Figure 10 for different combinations of substitution (S1−S8) and functional groups (R) that present two-electron reduction equilibria at pH = 0 (orange circles) and 7 (blue triangles). The reduction potential value of benzidine is also shown for comparative purposes. The number of derivatives with a dismutation process is greater at pH = 0 than at pH = 7. Derivatives exhibiting dismutation in the entire water pH window are enclosed in black, for instance, S3−R3 ($-OCH_3$) previously mentioned. However, there are derivatives where the stability window has a short pH range that still show bielectronic processes at pH = 0 and 7, as the S6−R9 ($-CF_3$) derivative.

In general, the derivatives shown in Figure 10 could work as posolytes in RFBs. However, given the redox potential difference observed, a further analysis of the possible catholyte/anolyte couples was performed. We found 22 pairs with a cell voltage between 0.50 and 0.60 V to operate a flow cell at pH = 0 (see the heatmap plot in Figure S14), where the pair S6−R3 ($-OCH_3$)/S7−R9 ($-CF_3$) has a larger cell voltage of 0.60 V. Furthermore, 15 couples were determined for a flow cell at pH = 7.0 with voltages in the range from 0.50 up to 0.68 V (Figure S15 in the Supporting Information). In this case, the couple S8−R3 ($-OCH_3$)/S7−R8 ($-NO_2$) is in the upper limit of 0.68 V.

## CONCLUSIONS

In this study, benzidine derivatives are proposed as electroactive compounds for organic redox flow batteries. The electrochemical characterization of the aqueous-soluble SDPAS dimer obtained by electrosynthesis was carried out. The experimental and theoretical Pourbaix diagram evidenced that, as well as benzidine, this compound has a bielectronic reduction process at acidic and basic pH values, while two monoelectronic reduction processes occur at a pH range from ca. 3 to 12. The stability diagnostic in an electrochemical flow cell of the SDPAS dimer as catholyte using phosphate buffer solution (1 mol $L^{-1}$, pH = 7) showed that the charge capacity is low after a relatively few cycles.

Both benzidine and the SDPAS dimer have single-electron-transfer processes unfavorable for the redox flow cell operation, such as variations in the cell voltage and a split in the total electrolyte capacity. Besides, the desired bielectronic process occurs at a very acidic pH (−1.1 to 2.0), making these conditions unattractive for cell handling.

To improve cell performance, we calculate the Pourbaix diagrams of benzidine derivatives and calibrate them with the experimental data of the SDPAS dimer. The theoretical PDs obtained allowed the identification of potential candidates with the following characteristics: (1) derivatives with a bielectronic process or small stability window of the radical species in the entire water pH window (0−14); (2) derivatives with a dismutation process below neutral pH (0−7) and a large stability window of the radical species beyond neutral pH. Although it is possible to identify a dismutation process at basic pH for some derivatives, its interpretation must be careful since experiments have demonstrated undesired species in this region.



https://doi.org/10.1021/acsomega.3c02297
ACS Omega 2023, 8, 32432−32443

The screening based on the PDs allowed the selection of 74 catholytes and possible anolytes at pH = 0 and 7. To generate a cell voltage between 0.50 and 0.68 V, 22 couples were found that can operate at pH 0, while another 15 could work at pH = 7. For instance, at pH = 0, the compound S6−R3 (−$OCH_3$ group), combined with the derivatives S7−R9 or S8−R8 (−$CF_3$ and −$NO_2$ functional groups, respectively), could generate a cell voltage close to 0.60 V. At pH = 7, the couple S8−R3 (−$OCH_3$)/S7−R8 (−$NO_2$) showed the highest cell voltage of 0.68 V. Therefore, this assessment can help to establish benzidine derivative couples for a full-organic aqueous redox flow battery.

## ■ ASSOCIATED CONTENT

### Supporting Information

The Supporting Information is available free of charge at https://pubs.acs.org/doi/10.1021/acsomega.3c02297.

Cyclic voltamperograms of the SDPAS monomer and the dimer obtained in a redox flow cell, chemically and by CV at different pH values, theoretical Pourbaix diagrams of benzidine and benzidine derivatives, as well as the cell voltage heatmap at pH values 0 and 7 (PDF)

## ■ AUTHOR INFORMATION


### Corresponding Authors

**Mariano Sánchez-Castellanos** − *Departamento de Física y Química Teórica, Facultad de Química, Universidad Nacional Autónoma de México, CDMX 04510, México;* orcid.org/0000-0003-0566-0975; Phone: +52 55 56223807; Email: msanchezcastellanos@quimica.unam.mx

**Víctor M. Ugalde-Saldívar** − *Departamento de Química Inorgánica, Facultad de Química, Universidad Nacional Autónoma de México, CDMX 04510, México;* orcid.org/0000-0002-9625-8713; Phone: +52 55 56223807; Email: vmus@unam.mx

### Authors

**Martha M. Flores-Leonar** − *Departamento de Física y Química Teórica, Facultad de Química, Universidad Nacional Autónoma de México, CDMX 04510, México;* orcid.org/0000-0002-2848-0478

**Gloria Acosta-Tejada** − *Departamento de Química Inorgánica, Facultad de Química, Universidad Nacional Autónoma de México, CDMX 04510, México;* orcid.org/0000-0002-9970-7027

**Humberto G. Laguna** − *Departamento de Química, Universidad Autónoma Metropolitana Iztapalapa, CDMX 09340, México;* orcid.org/0000-0002-5565-1551

**Carlos Amador-Bedolla** − *Departamento de Física y Química Teórica, Facultad de Química, Universidad Nacional Autónoma de México, CDMX 04510, México;* orcid.org/0000-0001-9590-2645

Complete contact information is available at: https://pubs.acs.org/10.1021/acsomega.3c02297


### Notes

The authors declare no competing financial interest.

## ■ ACKNOWLEDGMENTS

The authors thank DGTIC-UNAM for computational resources provided under project LANCAD-UNAM-DGTIC-022. This research was funded by CONACyT under project 292862. M.M.F.-L. thanks for the research funding provided under the program UNAM-DGAPA-PAPIIT IA206622. G.A.-T. thanks DGAPA-UNAM for a postdoctoral fellowship award. The authors thank Andrés Aguilar Granda and USAII FQUNAM for their support with the synthesis of the compounds and their $^1$H-NMR characterization.

## ■ REFERENCES


(1) Noack, J.; Roznyatovskaya, N.; Herr, T.; Fischer, P. The chemistry of redox-flow batteries. *Angew. Chem., Int. Ed.* **2015**, *54*, 9776−9809.

(2) Lourenssen, K.; Williams, J.; Ahmadpour, F.; Clemmer, R.; Tasnim, S. Vanadium redox flow batteries: A comprehensive review. *J. Energy Storage* **2019**, *25*, No. 100844.

(3) Liu, Y.; Chen, Q.; Sun, P.; Li, Y.; Yang, Z.; Xu, T. Organic electrolytes for aqueous organic flow batteries. *Mater.Today Energy* **2021**, *20*, No. 100634.

(4) Tang, L.; Leung, P.; Xu, Q.; Mohamed, M. R.; Dai, S.; Zhu, X.; Flox, C.; Shah, A. A. Future perspective on redox flow batteries: aqueous versus nonaqueous electrolytes. *Curr. Opin. Chem. Eng.* **2022**, *37*, No. 100833.

(5) Park, J.; Lee, Y.; Yun, D.; Kim, D.; Hwang, G.; Han, B.; Kim, Y.; Jung, J.; Jeon, J. A benzo[a]phenazine-based redox species with highly reversible two-electron reaction for aqueous organic redox flow batteries. *Electrochim. Acta* **2023**, *439*, No. 141644.

(6) Wu, M.; Bahari, M.; Fell, E. M.; Gordon, R. G.; Aziz, M. J. High-performance anthraquinone with potentially low cost for aqueous redox flow batteries. *J. Mater. Chem. A* **2021**, *9*, 26709−26716.

(7) Ambrose, B.; Naresh, R.; Kathiresan, M.; Ulaganathan, M.; Ragupathy, P. Highly Stable Asymmetric Viologen as an Anolyte for Aqueous Organic and Halide-Based Redox Flow Batteries. *Energy Technol.* **2023**, *11*, No. 2201046.

(8) Zhang, C.; Niu, Z.; Peng, S.; Ding, Y.; Zhang, L.; Guo, X.; Zhao, Y.; Yu, G. Phenothiazine-Based Organic Catholyte for High-Capacity and Long-Life Aqueous Redox Flow Batteries. *Adv. Mater.* **2019**, *31*, No. 1901052.

(9) Kosswattaarachchi, A. M.; Cook, T. R. Repurposing the Industrial Dye Methylene Blue as an Active Component for Redox Flow Batteries. *ChemElectroChem* **2018**, *5*, 3437−3442.

(10) Lai, Y. Y.; Li, X.; Liu, K.; Tung, W.-Y.; Cheng, C.-F.; Zhu, Y. Stable Low-Cost Organic Dye Anolyte for Aqueous Organic Redox Flow Battery. *ACS Appl. Energy Mater.* **2020**, *3*, 2290−2295.

(11) Mukhopadhyay, A.; Zhao, H.; Li, B.; Hamel, J.; Yang, Y.; Cao, D.; Natan, A.; Zhu, H. Abundant Organic Dye as an Anolyte for Aqueous Flow Battery with Multielectron Transfer. *ACS Appl. Energy Mater.* **2019**, *2*, 7425−7437.

(12) Martínez-González, E.; Amador-Bedolla, C.; Ugalde-Saldivar, V. M. Reversible Redox Chemistry in a Phenoxazine-Based Organic Compound: A Two-Electron Storage Negolyte for Alkaline Flow Batteries. *ACS Appl. Energy Mater.* **2022**, *5*, 14748−14759.

(13) Hong, J.; Kim, K. Neutral red and ferroin as reversible and rapid redox materials for redox flow batteries. *ChemSusChem* **2018**, *11*, 1866−1872.

(14) Bishop, E. *Indicators: International Series of Monographs in Analytical Chemistry*; Elsevier, 2013; Vol. *51*.

(15) Oldfield, L. F.; Bockris, J. O. Reversible Oxidation-Reduction Reactions of Aromatic Amines. *J. Phys. Chem. A* **1951**, *55*, 1255−1274.

(16) Won, M.-S.; Shim, Y.-B.; Park, S.-M. Electrochemical Oxidation of Benzidine and Hydrazobenzene. *Bull. Korean Chem. Soc.* **1992**, *13*, 680−683.

(17) Bishop, E.; Hartshorn, L. Some observations on oxidation-reduction indicators of the benzidine, naphthidine and diarylamine types. *Analyst* **1971**, *96*, 26−36.

(18) Hulanicki, A.; Głab, S. *Redox Indicators: Characteristics and Applications*; Pergamon, 1978.

(19) O'Boyle, N. M.; Banck, M.; James, C. A.; Morley, C.; Vandermeersch, T.; Hutchison, G. R. Open Babel: An Open Chemical Toolbox. *J. Cheminf.* **2011**, *3*, No. 33.

(20) Frisch, M. J.et al. *Gaussian 16*; revision C.01; Gaussian Inc.: Wallingford CT, 2016.
(21) Becke, A. D. Density-functional thermochemistry. III. The role of exact exchange. *J. Chem. Phys.* **1993**, *98*, 5648−5652.
(22) Marenich, A. V.; Cramer, C. J.; Truhlar, D. G. Universal Solvation Model Based on Solute Electron Density and on a Continuum Model of the Solvent Defined by the Bulk Dielectric Constant and Atomic Surface Tensions. *J. Phys. Chem. B* **2009**, *113*, 6378−6396.
(23) Rojas-Hernández, A.; Ramírez, M. T.; González, I.; Ibañez, J. G. Predominance-Zone Diagrams in Solution Chemistry: Dismutation Processes in Two-Component Systems (M-L). *J. Chem. Educ.* **1995**, *72*, No. 1099.
(24) Donald, W.; Leib, R.; O'Brien, J.; Williams, E. Directly Relating Gas-Phase Cluster Measurements to Solution-Phase Hydrolysis, the Absolute Standard Hydrogen Electrode Potential, and the Absolute Proton Solvation Energy. *Chem. - Eur. J.* **2009**, *15*, 5926−5934.
(25) Ishikawa, A.; Nakai, H. Quantum chemical approach for condensed-phase thermochemistry (III): Accurate evaluation of proton hydration energy and standard hydrogen electrode potential. *Chem. Phys. Lett.* **2016**, *650*, 159−164.
(26) Trasatti, S. The absolute electrode potential: an explanatory note (Recommendations 1986). *Pure Appl. Chem.* **1986**, *58*, 955−966.
(27) Rifi, M. The electrochemical oxidation of benzidine. *Tetrahedron Lett.* **1969**, *10*, 5089−5092.
(28) Rojas-Hernández, A.; Ramírez, M. T.; Ibáñez, J. G.; González, I. Construction of multicomponent pourbaix diagrams using generalized species. *J. Electrochem. Soc.* **1991**, *138*, 365−371.


https://doi.org/10.1021/acsomega.3c02297
*ACS Omega* 2023, 8, 32432−32443